

Experimental Verification of Theory of Landing Impact

By Walter Ramberg and Albert E. McPherson

Drop tests of an idealized wing and alighting gear were made to provide an experimental check on methods for computing the transient bending stresses in the wing produced by a symmetrical vertical landing impact. The model was dropped in a nearly strain-free condition to make contact at a point below the center of gravity. The forces in the alighting gear, acceleration at the "fuselage", and bending strains in the wing were recorded as a function of time.

According to the statistical theory of Biot and Bisplinghoff, the computed maximum bending stresses, using the first three flexural modes, were found to be 43 to 137 percent greater than the measured values. Using the actual forcing function reduced the difference to less than 20 percent.

I. Introduction

The tests described in this paper¹ were made for the Bureau of Aeronautics, United States Navy Department, to provide an experimental verification of analytical methods for determining the transient oscillations in the structure of an airplane during landing impact.

The practical importance of this problem for the safe operation of large airplanes has been stressed by Biot and Bisplinghoff [1]², Keller [2], and Yorgiadis [3].

The analysis of the transients during landing impact is complicated by the fact that these transients involve many natural modes of vibration of the airplane, and response in each mode depends on the force-time curve at the point of contact. The force-time curve will vary from one landing to the next of a given airplane. In view of these complications, Biot and Bisplinghoff proposed an ingenious statistical approach to the landing problem. In this approach the vibration of the structure in a given mode is reduced to that of an equivalent linear oscillator, and the maximum amplitude in that mode is estimated from an envelope of "dynamic response factors", which bounds the response to impact force-time

curves of any shape that may be expected in the landing. An upper limit to the resultant amplitude is obtained by adding up the maximum amplitudes in the various modes.

Application of Biot and Bisplinghoff's statistical approach involves the following assumptions, which may affect the accuracy of the result:

1. The maximum amplitude in the various modes is added up without regard to phase differences. This will lead to a resultant that may be considerably larger than the resultant when phase differences are taken into account.

2. The most severe impact force-time curve during the landing approaches in effect one of the impact force-time curves that were used by Biot and Bisplinghoff to derive their envelope of "dynamic response factors". Further measurements of landing impacts in service and of impact force-time curves in drop tests of landing gear may lead to modifications of the envelope of dynamic response factor. The envelope should be raised if service showed more severe impact force-time curves than those assumed by Biot and Bisplinghoff. It could be lowered if they were found to be consistently less severe.

3. It is sufficient to confine the analysis to the first few modes of vibration. Inclusion of modes of higher order than about the fifth is impracticable, because they are either unknown or too difficult to determine. This may lead to an exces-

¹ This paper was presented before the Sixth International Congress for Applied Mechanics in Paris on Sept. 27, 1946.

² Figures in brackets indicate the literature references at the end of this paper.

sively low value of the resultant if the higher modes contribute a significant proportion to the resultant.

4. The force-time curve at the landing gear is independent of the flexibility of the airplane structure. Actually there may be an appreciable coupling between the elastic deflection of the structure and the action of the landing gear.

5. The effect of damping is negligible. Damping may introduce coupling between the various modes of vibration of the airplane, thereby making it impossible to analyze the vibration in any given mode apart from that in all other modes.

6. Nonlinear effects are negligible. Nonlinear effects caused by buckling of the sheet, slipping of rivets, exceeding of the proportional limit of the materials in portions of the structure may introduce coupling between various modes.

II. Description of Model

1. Wing

The wing was designed to have a mass and flexural-rigidity distribution approximating that of a $\frac{1}{10}$ -scale model of a large military airplane. The assembled model is shown in figure 1. The wing was a tapered box beam of rectangular section. It was constructed of aluminum alloy sheet and angles fastened with $\frac{1}{8}$ -in. rivets. The nominal cross-sectional dimensions at several stations along the wing are shown in figure 2.

The flexural rigidity, EI , at various stations along the completed wing was computed from measurements of extreme fiber strains when the wing was subjected to a known bending moment. The results are given in figure 3.

The mass distribution of the wing was measured

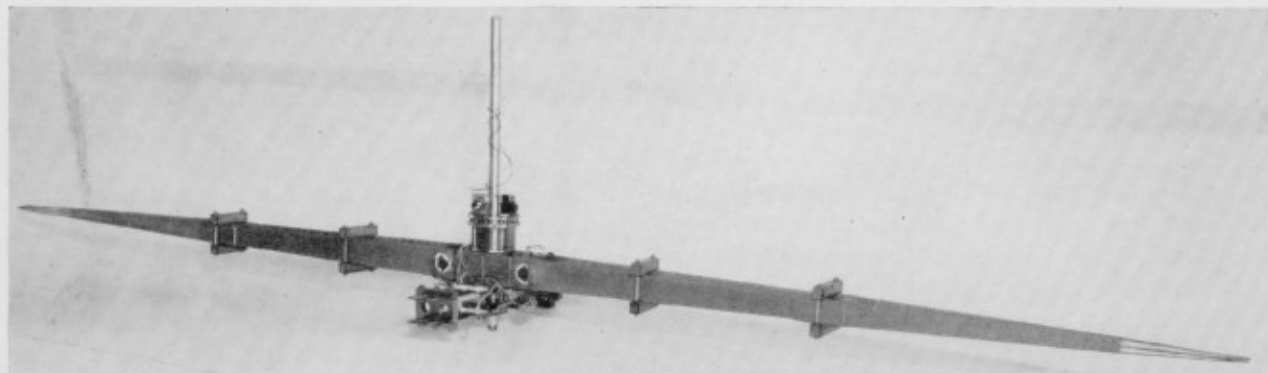


FIGURE 1. *Idealized model.*

An experimental verification of Biot and Bisplinghoff's analysis was decided upon in order to determine the adequacy of the assumptions and to indicate the minimum number of modes of vibration that must be included to estimate maximum bending moments and accelerations at various stations along the wing.

The experimental verification was started with the tests described in this paper. These tests are concerned with the simplest case, namely that of measuring the flexural transients in a symmetrically tapered model wing when the model is subjected to a vertical impact force directly below the center of gravity. Four engine masses were mounted symmetrically on the wing so as to subject it to bending without torsion during the landing impact.

by a volumetric method. This involved stripping the wing of the engine weights and measuring the change in weight as the wing was lowered into a large container of water. The measured values of mass per inch are shown in figure 4, a. Figure 4, b shows the magnitude and location of concentrated masses corresponding to the engines and fuselage.

2. Alighting Gear

(a) Damper

Adjustment of the damping force over a wide range was made possible with a fluid damper built into the center of the model. The damper, figures 5 and 6, consisted essentially of a piston forcing fluid out of 8 adjustable ports in a cylinder. The ports were located in the side of the cylinder

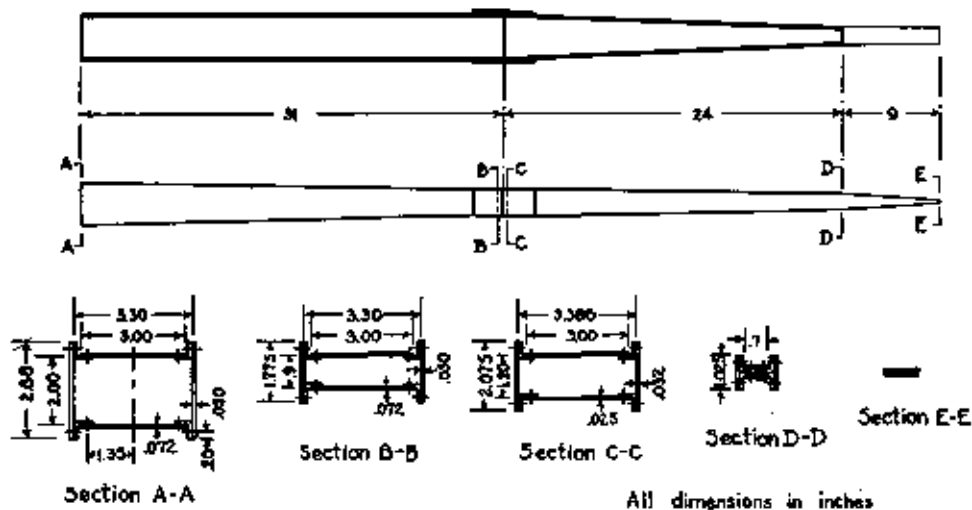


FIGURE 2. Nominal cross-sectional dimensions of model wing.

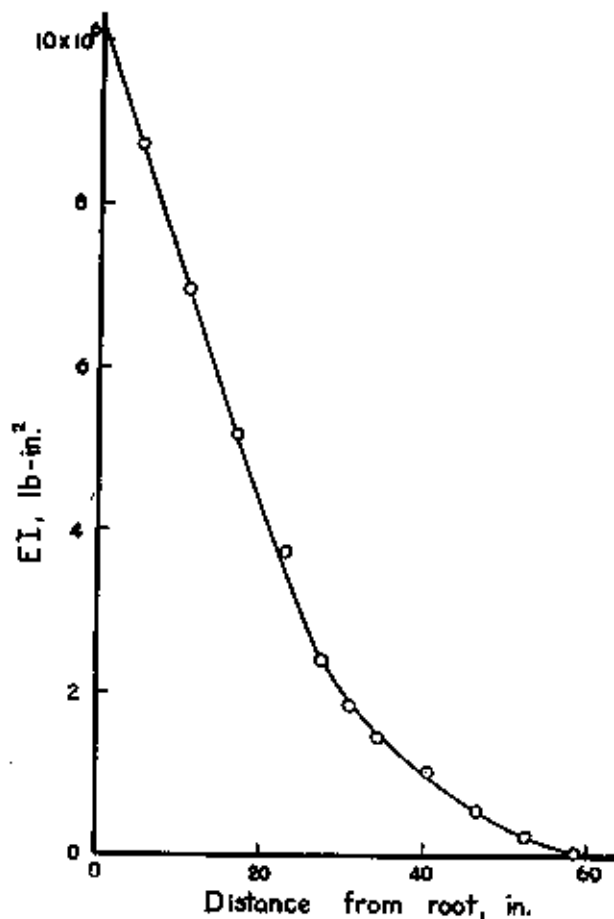


FIGURE 3. Flexural rigidity distribution for model wing.

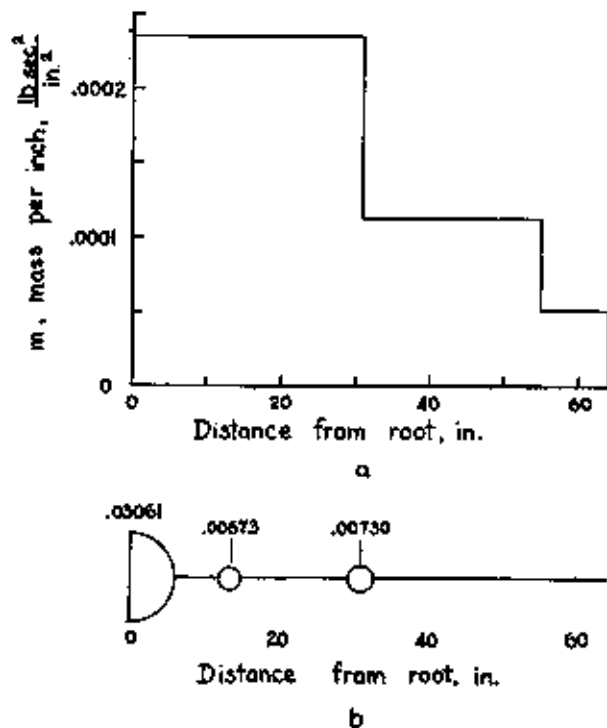


FIGURE 4. Mass distribution for model wing; a, distributed mass; b, concentrated mass, lb sec²/in².

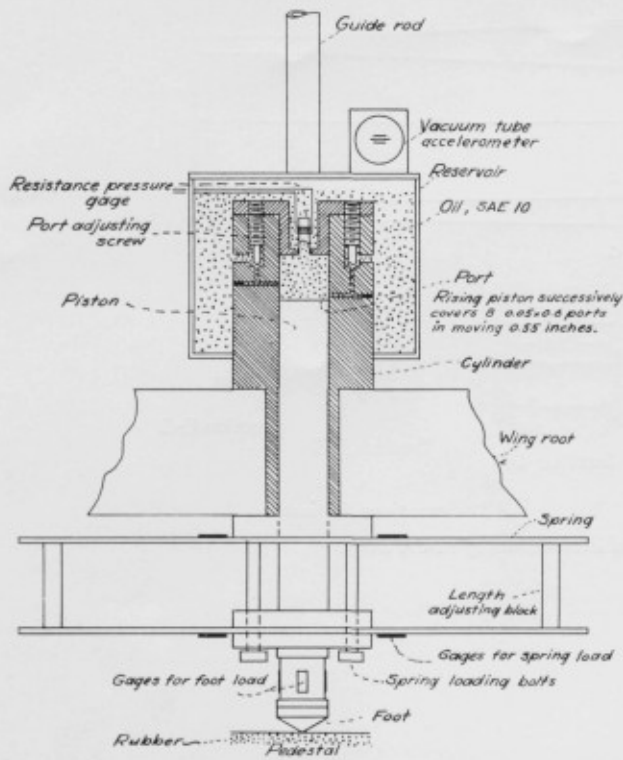


FIGURE 5. Schematic diagram of alighting gear.

wall at 0.07-in. intervals along the path of travel of the piston. As the piston traveled up the cylinder, it successively closed off the ports. The shape of the curve of damping force versus piston displacement could be changed by adjusting the initial opening of the various ports.

(b) Spring

The cushioning action of the air pressure in an oleo strut was approximated in the model by a pair of double cantilever springs shown near the bottom of figure 5. The springs were designed to have a wide range of adjustment of stiffness. The stiffness was changed by moving the length-adjusting block either closer or farther from the vertical centerline of the model. The springs were attached between the landing foot and the root of the model. The initial load applied by the spring between root and wing could be adjusted with the spring-loading bolts shown in figure 5.

(c) Landing Foot

The landing foot of the model is shown at the bottom of figures 5 and 6. It had a conical impact surface, which was intended to give a nonlinear force-displacement relation as the foot com-

pressed the rubber-surfaced landing pedestal. A nonlinear force-displacement relation was desired to simulate the nonlinear characteristics of the tire in an actual airplane. The shape of the force-displacement curve was varied by changing the thickness of the rubber and by using natural rubber, Neoprene, and combinations of the two.

III. Tests

1. Release Gear

The release gear shown in figure 7 was developed to drop the model in the nearly "strain-free condition" that should hold during free fall. This prevents the setting up of vibrations excited by the sudden removal of the dead-weight forces upon release of the model. It has been found that such vibrations may interfere seriously with the interpretation of the strains and accelerations recorded during drop tests of full-size airplanes.

The release gear supports the model at several stations along the wing with forces that are adjusted to be nearly in balance with the local dead-weight forces. Upon release, the supports are removed at an acceleration greater than gravity, thus leaving the model free to fall in its nearly strain-free condition.

The support is applied to the model by eight pointed screws, *B*, at the ends of six arms, *A*, figure 7. The screws, *B*, were carefully adjusted until strain gages attached to the model near the root and near the first engine indicated the model was in a "strain-free condition". Strain readings

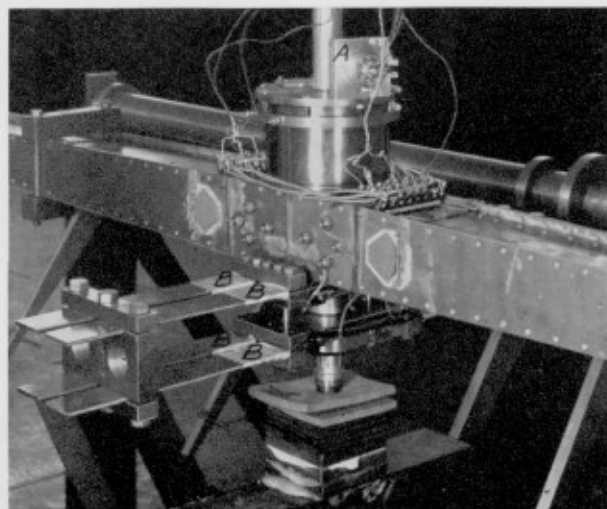


FIGURE 6. Center section of idealized model.

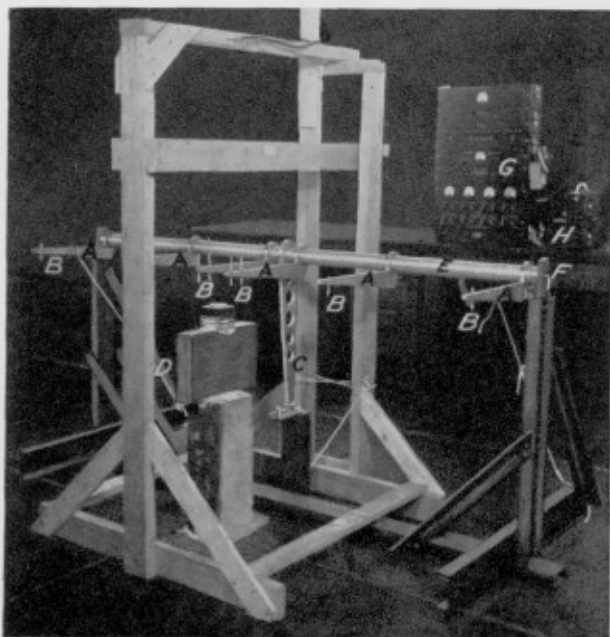


FIGURE 7. Release gear.

corresponding to the "strain-free" condition were determined as the average of readings for the $+g$ and the $-g$ condition. The $+g$ condition was obtained by holding the model above the center of gravity with the landing foot vertical below the center of gravity; the $-g$ condition was obtained by turning the model through 180° about the wing axis to place the landing foot vertically above the center of gravity.

The model was released by cutting an 0.04-in. steel wire attached to lever *C*, which held the release gear in the supporting position. The supports were swung away from under the model at an acceleration greater than g by heavy rubber bands, *D*, which rotated the main support rod, *E*, about ball bearings at the ends. A friction catch at *F* on rod *E* prevented the arms, *A*, from swinging back into the model.

2. Instrumentation

The instrumentation of the model included pick-ups for measuring bending moment near the fuselage and near the first outboard engine, acceleration at the fuselage, force transmitted through the springs, and force transmitted through the damper.

All quantities except acceleration were measured with pick-ups by using strain-sensitive wire. The signal of these pick-ups was amplified with the

four-channel equipment shown at *G* in figure 7. It was then recorded in the six-channel recorder, *H*. The amplifying equipment included in each channel a 1,000 c/s carrier-current Wheatstone bridge and a band-pass filter to give nearly flat response up to 100 c/s; at 200 c/s the response was down about 20 percent. The recorder was equipped with galvanometers having a natural frequency of 430 c/s and a response that was flat up to 100 c/s; the response rose about 20 percent at 200 c/s; it dropped off rapidly above 300 c/s.

Acceleration was measured with a vacuum-tube acceleration pick-up developed at the National Bureau of Standards. The pick-up contains two separate flexibly mounted plates on opposite sides of a fixed cathode. The plates are deflected elastically by the accelerations, thereby increasing the current between one plate and the cathode and decreasing it between the other plate and the cathode. The total change in current is recorded through a Wheatstone bridge. The pick-up has a fundamental frequency of about 800 c/s. The output was fed through a low-pass filter into the recorder, *H*, giving a flat response up to 200 c/s.

The bending moments at various stations on the wings were measured by attaching pairs of wire-strain gages to the top and bottom of the wing and connecting them in opposition in a Wheatstone bridge circuit so that the output was proportional to the extreme fiber-bending strain. In addition, gages in corresponding positions on the right and left halves of the wing were connected in series to average their output electrically. The over-all circuit from gages through Wheatstone bridge, amplifier, and oscillograph was calibrated statically before each set of drop tests by applying known bending moments to the wing and recording the output.

The acceleration at the fuselage was measured with the vacuum-tube acceleration pick-up, *A*, figure 6. The pick-up and circuit were calibrated with an acceleration of $2g$ applied before each set of drop tests by reversing the accelerometer in the earth's gravitational field and recording the output.

The force transmitted through the spring was measured by attaching wire-strain gages, *B*, figure 6, to each of the eight leaves of the spring and connecting them into a Wheatstone bridge circuit in such a way that their output was proportional

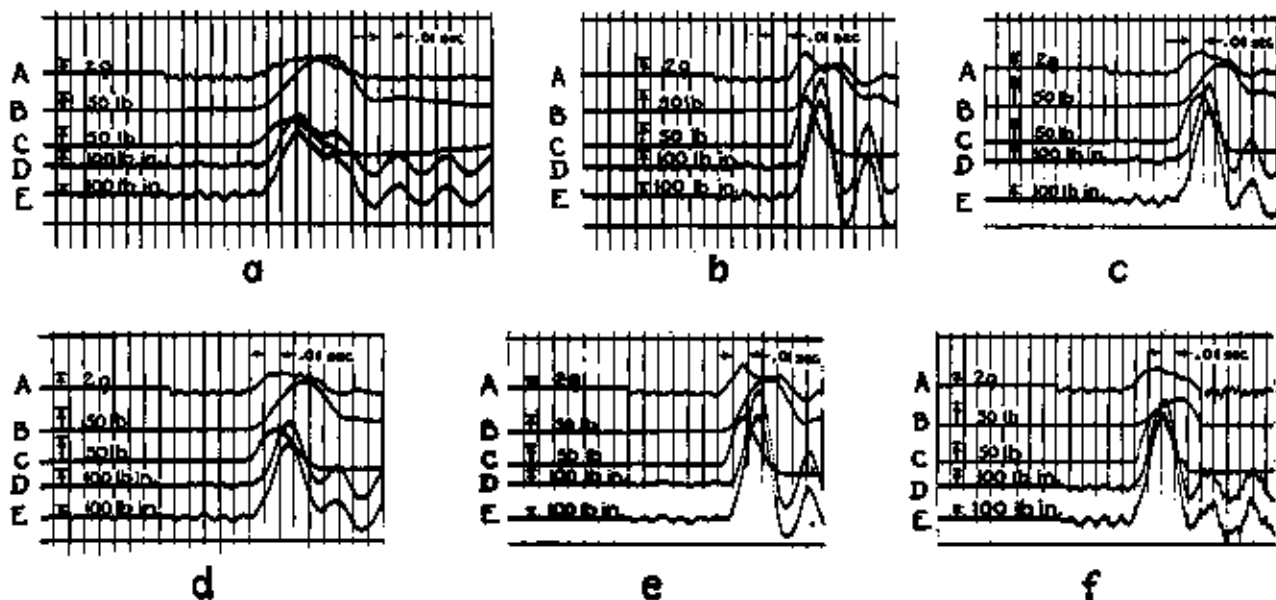


FIGURE 8. Drop tests from a height of about 0.7 in.

Pressure relief ports open $\frac{1}{4}$ turn in tests a to e. In test f, ports 1 to 5 open one-fourth turn, and parts 6 to 8 closed. A, inlet acceleration; B, spring; C, damper; D, outboard bending; E, root bending.

Test	Initial spring loading	Number of rubber pads under landing foot	
		Natural	Neoprene
a.....	0	5	0
b.....	0	0	2
c.....	0	2	2
d.....	0	2	4
e.....	0	1	4
f.....	43	2	4

to the total force transmitted by the spring. A static calibration was obtained before each set of tests by applying known forces and recording the output.

The force transmitted through the damper was measured by a small pressure gage at the top of the cylinder chamber, figure 5. This pressure gage consisted of an aluminum alloy tube $\frac{1}{2}$ -in. long, $\frac{3}{8}$ in. in diameter, and of 0.0035-in. wall thickness. The tube had one end closed and the other end open to the fluid in the cylinder. On the outside of the tube 0.001-in. constantan wire was wound and cemented into place taking care to insulate the wire from the tube and to bring out firmly anchored lead wires. A static calibration of the gage showed it to have a linear change in resistance with pressure up to pressures of 300

lb/in.², corresponding to forces of 500 lb transmitted through the damper.

IV. Results

The records showing the results of the drop tests from a height of about 0.7 in. are shown in figure 8. Six drops were made in which the landing conditions were varied by changing the softness of the rubber on which the model was dropped, the initial spring loading, and the opening of the pressure relief ports in the damper. The initial spring loading of 43 lb, for impact, (figure 8, f, corresponds to supporting the whole weight of the model on the springs.

The shortest impact, lasting about 0.050 sec, is shown in figure 8, f, and the longest impact, last-

ing about 0.086 sec, is shown in figure 8, a. The ratio of impact time to the period of the model in its fundamental bending mode approximately covers the range of this ratio for large airplanes.

The maximum observed bending moments in the wing at stations 1.5 in. and 14.5 in. from the root are given in table 1. In addition, table 1 gives the maximum observed accelerations at the root, the duration of the impact, and the maximum impact force. The maximum impact force was obtained as the maximum value of the sum of the forces transmitted through the springs and the damper.

TABLE 1. Maximum values of the applied impact force (sum of spring and damper forces), bending moments at 1.5-in. and 14.5-in. stations, and accelerations at root

Record	Maximum impact force per half wing	Bending moment $M_{l.s.}$		Maximum acceleration at root		Impact duration
		1.5-in.	14.5-in.	ft/sec^2	g	
a.....	95	780	370	1,582	4.1	0.086
b.....	105	1,130	690	1,932	5.0	.076
c.....	100	1,000	580	1,660	4.1	.083
d.....	93	970	540	1,610	3.9	.080
e.....	120	1,370	820	2,230	5.8	.082
f.....	113	1,170	600	1,920	4.2	.080

V. Analysis

1. Normal Modes of Vibration

The normal modes of vibration of the model wing in bending were computed by considering the mass to be concentrated at the root and at nine stations along each half-wing. The distributed

mass of the portion of the wing between adjacent stations was distributed to those stations in inverse proportion to the distance from each station to the center of gravity of the portion of wing being considered. The values are given in table 2. Influence coefficients were then computed between the mass points by treating each half-wing as a simple beam clamped at the root. The first three flexural modes of the wing in free-free vibration were computed from these influence coefficients and from the given mass distribution using a dynamic matrix and iteration procedure as explained by Duncan and Collar [4]; the deflection at the root of the wing was obtained from the condition that the center of gravity of the wing must remain at rest for free-free vibration. In the case of the second and third mode, the iteration procedure had to be modified to prevent convergence to the fundamental mode. This was accomplished by removing any proportion of lower modes present with the help of the orthogonality relations as outlined for propeller blades in [5].

The deflections in each mode r were normalized by dividing the deflection, $y_i^{(r)}$, at a given station, i , by that at the tip station. The values are given in table 2.

The normalized deflection, $\eta_i^{(r)}$, were substituted in the following formula to obtain the generalized mass, M_r , of the equivalent linear oscillator in mode r (see [1]):

$$M_r = \sum_{i=0}^9 m_i (\eta_i^{(r)})^2, \quad (1)$$

where m_i is the mass at station i . The values are given in table 3, together with the frequencies and periods in each mode.

TABLE 2. Distribution of mass and flexibility along half-wing and shape of natural modes

Station No.	Station, inches from root	Mass	Flexibility, $1/EI$	Normalized deflection in mode, v_1	Normalized deflection in mode, v_2	Normalized deflection in mode, v_3	Normalized deflection in mode, v_4
0.....	0	$lb-sec^2/in.$	$10^{-4}/lb-in.^2$				
1.....	6.5	0.03142	0.099	1	-0.08208	0.03531	-0.01834
2.....	13.5	.00161	.116	1	-.07089	.02330	-.00406
3.....	21.5	.00360	.162	1	-.03855	-.01493	.03395
4.....	31.0	.00206	.200	1	.02970	-.07756	.07631
5.....	41.0	.00099	.261	1	-.16044	-.13330	-.06838
6.....	41.0	.00106	.275	1	.33362	-.07606	-.13614
7.....	49.0	.000728	2.00	1	.62797	.03663	-.28679
8.....	63.5	.000510	5.15	1	.64232	.16102	-.29426
9.....	69.0	.000296	27.5	1	.80679	.49114	.06996
9.....	64.0	.000129	200	1	1.00000	1.00000	1.00000

TABLE 3. Natural period, generalized mass, and bending moment for each natural mode

Mode, r	ω	Period, T_r	Generalized mass, M_r	Bending moment at 1.5 in. for unit tip deflection, $(M_{b,1.5})_r$		Bending moment at 14.5 in. for unit tip deflection, $(M_{b,14.5})_r$	
				lb-sec/in. tip	lb-in.	lb-sec/in. tip	lb-in.
0	0	0	0.055292	0	0	0	0
1	199.48	0.0315	.001322	4,421	3,071		
2	544.50	.01153	.000497	-6,213	-1,763		
3	1,026.06	.00613	.000315	7,238	-604		

Table 3 shows also the bending moments per unit-tip deflection in each mode at the two stations, 1.5 and 14.5 in. from the root, at which measurements were made. The bending moments were computed by considering the wing to be loaded at stations $i=1, 2, \dots, 9$ by transverse forces $\omega_r^2 m_i \eta_i^{(r)}$ where ω_r is the frequency in the r th mode.

2. Dynamic Response According to Theory of Biot and Bisplinghoff

The dynamic response of the model wing was computed by using Biot and Bisplinghoff's theory [1] for each of the 6 impacts shown in figure 9. These were obtained from the records of figure 8 by adding the spring and damper forces shown as B and C and dividing by 2.

(a) Bending Moment

The maximum bending moments $M_{b,1.5}$ and $M_{b,14.5}$ at stations 1.5 in. and 14.5 in. from the root were computed by adding up the maximum bending moments $(M_{b,1.5})_r$ and $(M_{b,14.5})_r$ for the first 3 modes $r=1, 2, 3$. Two sets of values were computed, the first an upper limit corresponding to the envelope of dynamic response factors γ_r given in figure 13 of [1], and the second a closer approximation corresponding to the response factor for that impact in figure 12 of [1] that came closest to the actual impacts shown in figure 9.

The bending moments in each mode r were obtained by multiplying the bending moments per unit tip deflection in table 3 by the tip deflection $\gamma_r Q_r / M_r \omega_r^2$, where Q_r is the generalized force in mode r . The generalized force was computed as the product of the maximum observed impact force and the normalized deflection at the root in mode r .

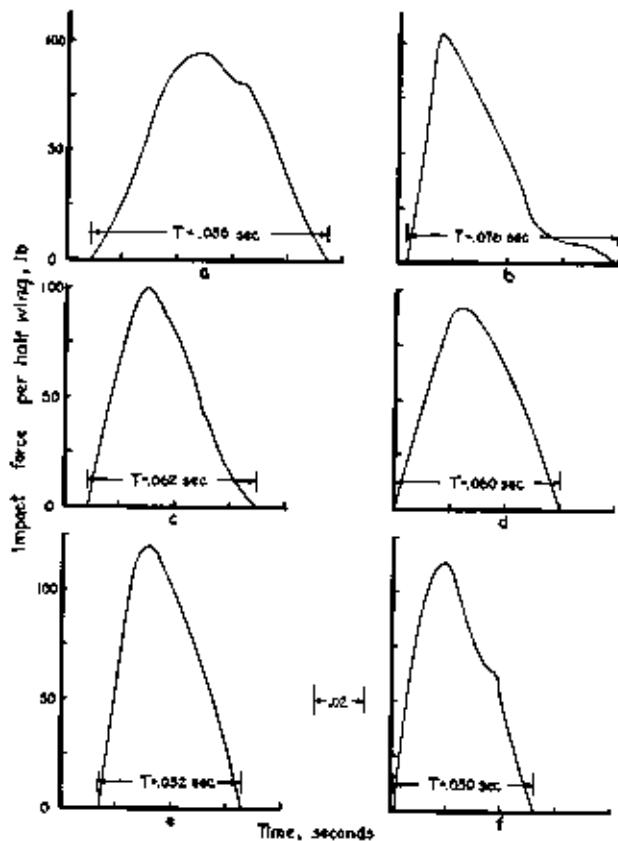


FIGURE 9. Total impact force per half wing for tests of figure 8.

TABLE 4. Bending moments according to theory of Biot and Bisplinghoff, lb-in.

Bending moments	Drop					
	a	b	c	d	e	f
$(M_{b,1.5})_1$ 1 envelope	-1,170	-1,321	-1,278	-1,182	-1,550	-1,460
$(M_{b,1.5})_2$ 2 envelope	-231	-270	-275	-256	-348	-331
$(M_{b,1.5})_3$ 3 envelope	-38	-42	-46	-43	-63	-60
$(M_{b,1.5})_1$ 1 best fit	-735	-1,173	-673	-650	-909	-925
$(M_{b,1.5})_2$ 2 best fit	-192	-203	-163	-175	-242	-226
$(M_{b,1.5})_3$ 3 best fit	-38	-43	-40	-37	-49	-47
$(M_{b,14.5})_1$ 1 envelope	-613	-918	-888	-821	-1,077	-1,014
$(M_{b,14.5})_2$ 2 envelope	-65	-77	-78	-73	-99	-94
$(M_{b,14.5})_3$ 3 envelope	3	3	4	4	5	5
$(M_{b,14.5})_1$ 1 best fit	-511	-815	-467	-451	-673	-644
$(M_{b,14.5})_2$ 2 best fit	-72	-68	-52	-50	-69	-64
$(M_{b,14.5})_3$ 3 best fit	3	3	3	3	4	4
$(M_{b,1.5})_1$ envelope	-1,439	-1,633	-1,609	-1,481	-1,962	-1,861
$(M_{b,14.5})_1$ envelope	-875	-992	-962	-890	-1,171	-1,103
$(M_{b,1.5})_1$ best fit	-966	-1,418	-896	-862	-1,260	-1,201
$(M_{b,14.5})_1$ best fit	-590	-870	-516	-498	-738	-704

The results of the computations are given in table 4. Examination of this table shows that the third flexural mode contributes less than 4 percent to the bending moment at the two stations. In view of this rapid convergence, it would have been sufficient in this particular case to confine the analysis to the first two flexural modes.

Comparison of the maximum bending moments computed, table 4, with those observed experimentally, table 1, shows that the computed values using the best fit impact curve are from 15 percent less to 51 percent more than those observed, and using the envelope impact curve are from 43 to 137 percent more than those observed.

(b) Acceleration at Root of Wing

A dynamic response factor α for acceleration, analogous to the dynamic response factor γ for deflections as given in figure 13 of [1], was determined as follows:

From equations (I-8) and (I-10) of [1],

$$\ddot{y}_{tip}^{(r)}(t) = \frac{Q_r(t)}{M_r} - \frac{\omega_r}{M_r} \int_0^t Q_r(\tau) \sin \omega_r(t-\tau) d\tau, \quad (2)$$

where

- $\ddot{y}_{tip}^{(r)}(t)$ = acceleration in mode r at tip
- $Q_r(t)$ = generalized force in mode r as a function of time
- τ = variable of integration
- t = time.

If we denote by Q_r the maximum value of $Q_r(t)$ and let $p_r(t)$ be a unit impact force defined by

$$p_r(t) = \frac{1}{Q_r} Q_r(t), \quad (3)$$

we obtain the dynamic response factor $\alpha^{(r)}(t)$ for acceleration as

$$\alpha^{(r)}(t) = \frac{\ddot{y}_{tip}^{(r)}(t)}{Q_r/M_r} = p_r(t) - \omega_r \int_0^t p_r(\tau) \sin \omega_r(t-\tau) d\tau. \quad (4)$$

The dynamic response factor $\alpha^{(r)}(t)$ can be considered as the ratio of the actual acceleration $\ddot{y}_{tip}^{(r)}(t)$ at the tip to the steady acceleration resulting from applying the peak generalized force Q_r to the generalized mass M_r .

The value of $\alpha^{(r)}(t)$ was evaluated for impacts of triangular shape and sinusoidal shape by using the analyses presented in eq 16 to 19 of [6]. The

peak values α of $\alpha^{(r)}(t)$ are plotted in figure 10 as a function of the ratio of impact pulse period T to mode period $T_r = 2\pi/\omega_r$. The dynamic response factor α for acceleration decreases rapidly as the ratio T/T_r is increased above 0.8. For T/T_r greater than 7, α is less than 0.20. As T/T_r approaches zero, α approaches 1.

The maximum acceleration \ddot{y}_0 at the root of the wing was computed by adding up the maximum accelerations $\ddot{y}_0^{(r)}$ for the first four modes $r=0, 1, 2, 3$, where $r=0$ corresponds to motion as a rigid body. Two sets of values were computed, as in the case of the bending moments, the first corresponding to the envelope of dynamic response factors α in figure 10 and the second corresponding to that one of the two shapes of the curve of impact force versus time, assumed for figure 10, that comes closest to the actual impact shown in figure 9.

The accelerations $\ddot{y}_0^{(r)}$ in each mode were obtained from

$$\ddot{y}_0^{(r)} = \frac{\alpha Q_r \eta_0^{(r)}}{M_r}, \quad (5)$$

where $\eta_0^{(r)}$ is the normalized deflection at the root. For the rigid body mode $r=0$,

$$\ddot{y}_0^{(0)} = Q_0/M_0, \quad (5a)$$

where Q_0 is one-half of the maximum impact force applied, and M_0 is one-half of the mass of the wing.

The results of the computation are given in table 5. Examination of table 5 shows that the second and third flexural modes contribute less than 4 percent to the acceleration at the root. It would have been sufficient in this case to con-

TABLE 5. Acceleration at root of wing according to theory of Eriot and Biplinghoff in./sec²

Acceleration	Drop					
	a	b	c	d	e	f
$\ddot{y}_0^{(0)}$	1,720	1,900	1,810	1,665	2,172	2,048
$\ddot{y}_0^{(1)}$ (envelope) ..	214	267	279	259	397	367
$\ddot{y}_0^{(2)}$ (envelope) ..	52	63	74	69	105	102
$\ddot{y}_0^{(3)}$ (envelope) ..	9	12	14	14	21	20
$\ddot{y}_0^{(1)}$ (best fit) ..	182	132	78	80	201	217
$\ddot{y}_0^{(2)}$ (best fit) ..	29	43	48	62	86	42
$\ddot{y}_0^{(3)}$ (best fit) ..	3	6	4	4	11	6
\ddot{y}_0 (envelope) ..	1,995	2,232	2,177	2,007	2,666	2,525
\ddot{y}_0 (best fit) ..	1,932	2,081	1,940	1,811	2,440	2,310

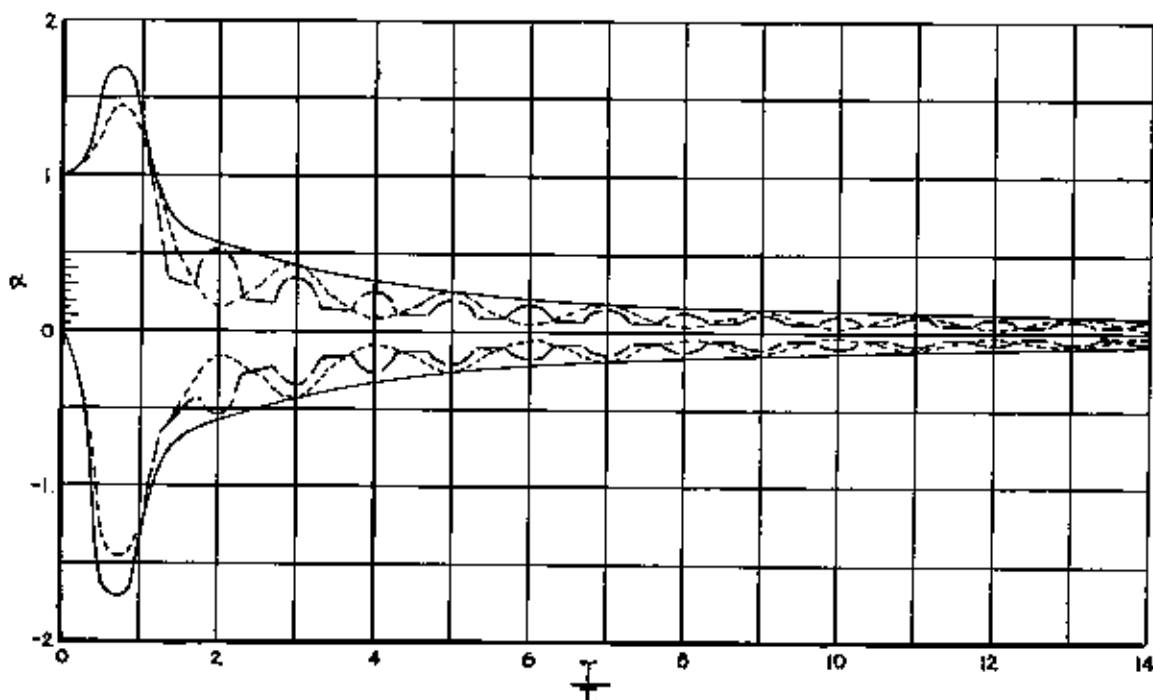


FIGURE 10. Dynamic response factor for acceleration.

--- Triangular pulse; - · - · sinusoidal pulse; ———, envelope.

fine the analysis to the rigid body motion and the fundamental flexural mode.

Comparison of the maximum computed accelerations at the root, table 5, with those observed experimentally, table 1, shows that the computed values using the envelope curve are from 16 to 56 percent more than those observed and, using the best fit curve, are from 8 to 43 percent more than those observed.

3. More Exact Analysis, Including Effect of Phase Differences

A basic assumption in the theory of [1] is that the maximum response of the wing in each mode may be added without regard for phase. The resulting error was computed by making a more exact analysis for the impact-time relation shown in figure 9, d.

The tip deflection in mode r ($r=1, 2, 3$) was computed from eq (I-10) of [1]

$$y_{tip}^{(r)} = \frac{1}{M_r \omega_r} \int_0^t Q_r(\tau) \sin \omega_r(t-\tau) d\tau, \quad (8)$$

where $Q_r(t)$ is the generalized force in mode r computed by multiplying the impact force-time

relation figure 9, d by the normalized deflection at the root, $\eta_0^{(r)}$. The integrations were carried out numerically. The resulting tip deflections in each of the first three flexural modes are shown in figure 11, a.

The bending moments $M_{s, 1.5}$ at 1.5 in. from the root were computed by multiplying the tip deflections in each mode by the corresponding factor in table 3. The resulting bending moments in each of the first three modes and their sum, as well as the observed bending moment, are shown in figure 11, b. Figure 11, c shows corresponding values at 14.5 in. from the root.

The acceleration at the root in the rigid body mode $r=0$ was computed from eq 5a after replacing Q_0 by $Q_0(t)$. The acceleration in the flexural modes $r=1, 2, 3$ was obtained from

$$\ddot{y}_0^{(r)} = \ddot{y}_{tip}^{(r)} \eta_0^{(r)} = \left[\frac{Q_r(t)}{M_r} - \omega_r^2 y_{tip}^{(r)} \right] \eta_0^{(r)}, \quad (7)$$

where $y_{tip}^{(r)}$ is the tip deflection given in figure 11, a. The results of the computation are given in figure 11, d, together with the observed acceleration at the root.

Examination of figures 11, b to 11, d shows that the observed maximum bending moments

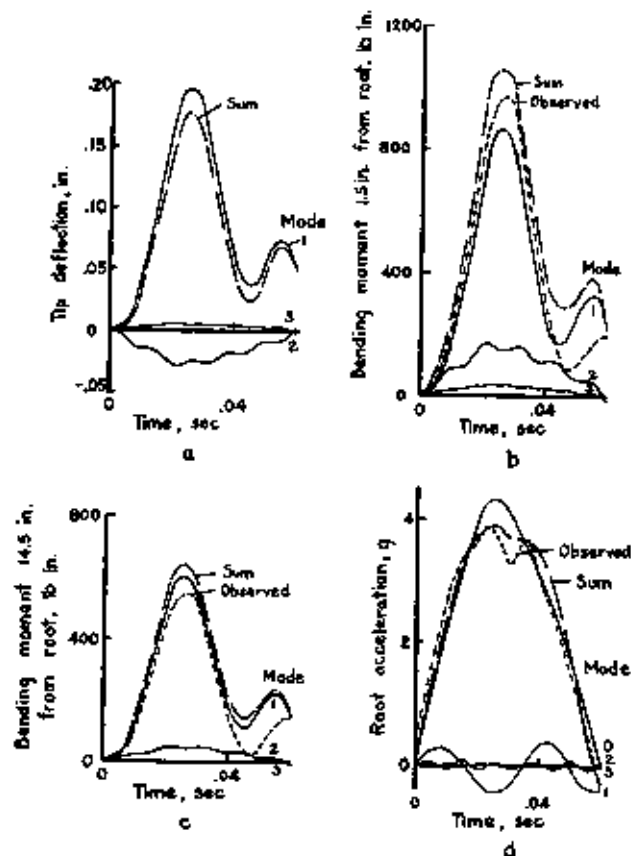


FIGURE 11. Detailed analysis for the impact force-time relation in figure 9,d.

and accelerations differed less than 20 percent from the computed values, when the phase differences were taken into account and when the actual impact force-time curve was used.

Comparison of the response in the individual modes in figure 11 shows that the error caused by neglecting phase differences was negligible (less than 1%) in the case of bending moments. In the case of acceleration at the root, the error was about 23 percent.

The good agreement observed for bending moment is primarily the result of the following two factors.

In aircraft structures (or models simulating aircraft), the periods of natural vibration T , are as short or shorter than the duration of the impact T . In such a case, a maximum bending moment and deflection response in all the modes occurs in phase at a time a little later than the maximum applied impact force. The response in the different modes drops off rapidly as the number of the

mode increases. Hence the contribution of the higher modes becomes negligible.

The phase difference can be important in the case of acceleration, as the acceleration in the first flexural mode may be, and in this example was, opposed in phase to that of the rigid body motion at the peak. Neglect of phase in the case of acceleration near the tip of the wing would probably lead to results so inaccurate as to be useless.

VI. Summary

An experimental verification of Biot and Bisplinghoff's analysis of landing impact is presented. An airplane model was built having a distribution of mass and of flexural rigidity along the wing approximately proportional to that for a four-engine military airplane. The four engine masses were mounted symmetrically on the wing so as to excite flexural vibrations without torsion when the model was dropped vertically to receive a landing impact below the center of gravity. The model contained an alighting gear with means for adjusting the time history of the impact force acting on the wings. Measurements were made of impact force, bending moments at two stations, and root acceleration for six landing conditions.

The observed maximum bending moments were compared with those computed by Biot and Bisplinghoff's method. The computed bending moment, using a response factor given by an envelope curve due to Biot and Bisplinghoff, was 43 to 137 percent larger than the observed bending moment. Use of an approximation to the actual impact-time relation gave bending moments from 15 percent less to 51 percent greater than the observed bending moments.

A more exact analysis, taking account of phase differences was made for one of the actual impact force-time curves. This gave maximum bending moments that differed less than 20 percent from the observed bending moments. Comparison of the computed response in the individual modes showed that the neglect of phase differences between the different modes, in accordance with Biot and Bisplinghoff's analysis, would have caused an error in maximum bending moment of less than 1 percent.

The observed maximum accelerations at the wing root were compared with those computed from an extension of Biot and Bisplinghoff's anal-

ysis, which involved the computation of response factor curves for acceleration. The computed acceleration, using a response factor given by the envelope to these curves, was 16 to 56 percent greater than the measured acceleration. Use of the most closely fitting impact curve reduced this error to 8 to 43 percent. It should be noted in this connection that larger differences may be expected at the wing tips, since these are more affected by flexural vibrations.

The more exact analysis for one of the impacts showed that the neglect of phase differences caused an error in computed maximum accelerations at the root of about 23 percent. This error would probably be much greater for acceleration at the wing tip.

The authors thank their colleagues Samuel Levy, for the analysis reported in this paper, and Eileen

D. Segal, for the numerical computations of dynamic response.

VII. References

- [1] M. A. Biot and R. L. Bisplinghoff, Dynamic loads on airplane structures during landing, NACA Wartime Report W-92 (Oct. 1944).
- [2] E. G. Keller, *J. App. Mech.* **11**, No. 4, A-219 to A-223 (1944).
- [3] Alexander J. Yorgiadis, *J. Inst. Aero. Sci.* **12**, No. 4, 421 (1944).
- [4] W. J. Duncan and A. R. Collar, *Phil. Mag. Ser. 7*, [17], No. 115, 866 (1934).
- [5] Walter Ramberg and Samuel Levy, *NBS J. Research* **31**, 639 (1938) RP 1148.
- [6] J. M. Frankland, Effects of impact on simple elastic structures, David W. Taylor Model Basin, Report 481 (1942).

WASHINGTON, July 9, 1948.